Biochemistry

Article

Cite This: Biochemistry 2017, 56, 5931-5942

pubs.acs.org/biochemistry

The G126V Mutation in the Mouse Prion Protein Hinders Nucleation-Dependent Fibril Formation by Slowing Initial Fibril Growth and by Increasing the Critical Concentration

Ambadi Thody Sabareesan and Jayant B. Udgaonkar*

National Centre for Biological Sciences, Tata Institute of Fundamental Research, Bengaluru 560065, India

Supporting Information

ABSTRACT: The middle disordered hydrophobic region of the prion protein plays a critical role in conformational conversion of the protein, with pathogenic as well as protective mutations being localized to this region. In particular, it has been shown that the G127V mutation in this region of the human prion protein (huPrP) is protective against the spread of prion disease, but the mechanism of protection remains unknown. In this study, quantitative analyses of the kinetics of fibril formation by wild-type mouse prion protein (moPrP) and G126V moPrP (equivalent to G127V huPrP) reveal important differences: the critical concentration is higher, the lag phase is longer, and the initial effective rate constant of fibril growth is slower for the mutant variant. The study offers a simple biophysical explanation for why the G127V mutation in huPrP would be protective in humans: the ∼5-fold increase in critical concentration caused by the mutation likely results in the critical concentration (below which fibril formation cannot occur) being higher that the concentration of the protein present in and on cells *in vivo*.

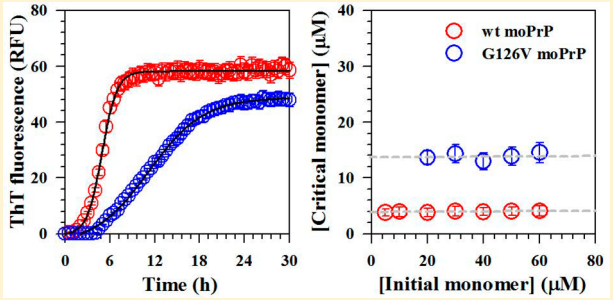

The prion diseases, also known as transmissible spongiform encephalopathies, are neurodegenerative disorders affecting mammals, including humans,[1] invariably with fatal consequences. In all prion diseases, the cellular prion protein (PrP^C) undergoes a conformational conversion into a misfolded and aggregated form (PrP^{Sc}). PrP^C has an unstructured N-terminal region (NTR) (residues 23−120) and a structured C-terminal domain (CTD) (residues 121−231).[2] The structure of PrP^{Sc} remains poorly understood. Although conformational conversion plays a crucial role in prion diseases, its mechanism remains unclear.

Typically, prion diseases are found to occur spontaneously or because of transmission from diseased individuals.[3] Nevertheless, prion disease can also occur due to inherited mutations in the *Prnp* gene, which encodes the prion protein.[4] These disease-causing mutations are found mainly in the middle hydrophobic core region (sequence segment 105−130) of the unstructured NTR, as well as in helix 2 (α2) and helix 3 (α3) of the structured CTD.[4] The occurrence of pathogenic mutations in the middle hydrophobic region is not surprising, given that it plays an important role in conformational conversion,[5,6] and in the assembly of misfolded fibrillar aggregates.[7−9]

Surprisingly, however, a novel protective mutation found in humans, G127V, in the same middle hydrophobic region, prevents individuals from being infected with prion disease.[10] Transgenic mice expressing the G127V human prion protein variant were found to be completely resistant to infection from all prion strains.[11] A recent molecular dynamics study of truncated prion protein has suggested that the G127V mutation weakens the main-chain H-bond interactions and prevents the formation of a dimer and a stable fibril core,[12] but this study lacks experimental verification. Understanding how the G127V mutation plays a protective role against infection is expected to afford a better understanding of how the prion protein undergoes conformational conversion and fibril formation.

Under *in vitro* conditions, amyloid fibril formation by recombinant prion protein is a good paradigm for understanding the mechanism of conformational conversion.[13,14] At low pH, and in the presence of salt, the prion protein can misfold and form oligomers, and these oligomers can associate and form wormlike amyloid fibrils.[15] In contrast, at physiological pH, the prion protein can be made to aggregate in the presence of chemical denaturants, to form long straight amyloid fibrils.[13,16,17] Aggregates generated *in vitro* from recombinant prion protein are very often cytotoxic,[18,19] but they may not be as infectious as aggregates isolated from diseased brains.[20,21] Nevertheless, *in vitro*-generated aggregates, despite being very difficult to generate, are known to spread disease in healthy organisms.[21,22] Consequently, the protective role of the protective mutation may be understood by studying its effect on the mechanism of amyloid fibril formation by recombinant prion protein.

The unusual capability of PrP^{Sc} to act as an infectious agent and propagate the disease, by interacting with PrP^C, suggests

Received: September 8, 2017
Revised: October 17, 2017
Published: October 18, 2017

DOI: 10.1021/acs.biochem.7b00894
Biochemistry 2017, 56, 5931−5942

that the mechanism of prion protein misfolding and aggregation could be very similar to that of nucleation-dependent polymerization (NDP).[23,24] Indeed, the amyloid fibril reactions of many recombinant proteins have been described by a NDP mechanism.[25−30] The amyloid fibril reaction of only the Y145 stop mutant variant of the prion protein has been described as NDP.[31] It is not known whether the full protein or even the C-terminal domain, which is commonly used as a proxy for the full protein, follows a NDP mechanism.

The mouse prion protein (moPrP) is useful for studying the effects of disease-linked mutations found in the human prion protein (huPrP).[13,20,32−36] Prion protein sequences are highly conserved across all mammals, with moPrP and huPrP having ∼85% identical sequences. In the middle hydrophobic region (residues 105−130; mouse numbering), the level of sequence identity is even higher. It is therefore very likely that the G126V mutation in moPrP will have the same effect as the G127V mutation in huPrP (residue number *n* in moPrP is equivalent to residue number *n* + 1 in huPrP). Wild-type (wt) moPrP has Met at residue position 128; hence, G126V moPrP (with V126 and M128) can be expected to display protective behavior similar to that shown by the huPrP variant (with V127 and M129) that is most protective.[11]

Here, an extensive study of the kinetics of fibril formation by wt moPrP and G126V moPrP has been performed over a wide range of protein concentrations. The defining features of a NDP mechanism are found to be met: sigmoidal kinetics with distinct lag, exponential, and stationary phases; abolition of the lag phase upon addition of preformed fibrils (seeds); and a critical concentration below which fibril formation cannot take place. The kinetics of fibril formation by G126V moPrP is different from that of wt moPrP in there being a higher critical concentration, a longer lag phase, and a decreased rate of fibril formation. The aggregation kinetics of wt and G126V moPrP were analyzed quantitatively, to show that the critical nucleus is monomeric. wt moPrP forms fibrils via a homogeneous nucleation pathway, whereas for G126V moPrP, secondary processes are also operative. Cross-seeding and co-aggregation experiments with wt and G126V moPrP monomer and fibrils suggest that the mutation affects the ability of the wt and mutant variant proteins to interact, both at the fibril−monomer level and at the monomer−monomer level.

MATERIALS AND METHODS

Buffers and Reagents. Chemical reagents and buffers of the highest purity grade were procured from Sigma-Aldrich. Guanidine hydrochloride, GdnHCl (molecular biology grade), was obtained from HiMedia.

Protein Expression and Purification. wt and G126V moPrP were expressed and purified as described previously.[15] The purified protein was subjected to a treatment to remove any very small amount of oligomer that escaped detection by dynamic light scattering. This treatment consisted of first incubating the protein in 8 M urea at pH 4 and 25 °C for 1 h to denature any possible aggregates present. The protein was then refolded in 10 mM sodium acetate (pH 4) buffer using a Sephadex G-25 HiTrap desalting column with an Akta Basic high-performance liquid chromatography instrument.

Far-Ultraviolet (far-UV) Circular Dichroism (CD) Measurements. Far-UV CD measurements were taken on a Jasco J-815 CD spectropolarimeter. A quartz cuvette with a path length of 1 mm and a protein concentration of 10 μM were used. The following instrument parameters were set: digital integration time, 2 s; bandwidth, 1 nm; scanning rate, 50 nm/min; wavelength scan, 200−250 nm.

Denaturant-Induced Equilibrium Unfolding Studies. For GdnHCl-induced equilibrium unfolding studies performed at pH 7 (in 50 mM Tris-HCl buffer), protein (10 μM) was incubated in different concentrations of GdnHCl for 2 h at 25 °C. The change in the far-UV ellipticity at 222 nm was monitored using the Jasco J-815 spectropolarimeter. Thermodynamic parameters were determined by fitting the data to a two-state (N ↔ U) unfolding model.[37] For full-length moPrP, it is the unfolding transition of the structured CTD of the protein[38] that is measured.

Fibril Formation of the Mouse Prion Protein. Fibril formation of moPrP was performed in 96-well plates in a Fluoroskan Ascent Microplate Fluorometer (Thermo Fisher Scientific Inc.). Before the start of the fibril formation reaction, the protein in 10 mM sodium acetate buffer (pH 4) was concentrated to ≈1.2 mM, using an Ultracel-3 3 kDa cutoff membrane (Millipore Inc.) placed in an Amicon Ultra 0.5 mL centricon filter unit. The protein stock was diluted 4-fold with unfolding buffer [65 mM Tris-HCl and 8 M GdnHCl (pH 7.4)], so that the protein (300 μM) was finally in 50 mM Tris-HCl and 6 M GdnHCl (pH 7.4), the final protein concentration. To start fibrillization, the protein in 3× fibrillization buffer [300 μM moPrP in 50 mM Tris-HCl and 6 M GdnHCl (pH 7.4)] was diluted with native buffer [50 mM Tris-HCl (pH 7.4)] so that the protein was finally in 1× fibrillization buffer [50 mM Tris-HCl and 2 M GdnHCl (pH 7.4)]. For all the reactions, thioflavin T (ThT) was added to a concentration equal to that of the protein concentration; 200 μL aliquots of the protein in 1× fibrillization buffer were then transferred to different wells of a 96-well plate, which was incubated at 37 °C and shaken at 480 rpm using the Fluoroskan Ascent Microplate Fluorometer. The ThT fluorescence was measured at 475 nm, upon excitation at 440 nm. The readings were acquired every 10 min.

Thioflavin T Fluorescence Assay. In the case of fibrillization reactions performed in the absence of ThT, an aliquot of protein, the volume of which was determined according to the concentration desired to be used for the experiment, was taken from the sample at different times of aggregation and added to the ThT assay solution [25 mM Tris-HCl (pH 7.4)]. The final concentrations of protein and ThT are 1 and 10 μM, respectively. Fluorescence was measured within 20 s of the addition of protein to the ThT solution, using a Fluoromax-3 spectrofluorometer (Jobin Yvon) with the excitation and emission wavelengths set at 440 and 482 nm, respectively, and the excitation and emission bandwidths set at 1 and 10 nm, respectively. The signal was averaged for 30 s, with a response time of 2 s.

Sedimentation Assays for Fibril Formation. At different times during fibril formation, a 100 μL aliquot was taken into a 1.5 mL microcentrifuge vial, which was centrifuged at 20000*g* for 45 min at 25 °C. The amount of protein present in the supernatant was determined by measuring the tryptophan fluorescence at 357 nm, upon excitation at 295 nm. The amount of protein present in aggregate form (the pellet) was then determined by subtracting the supernatant protein concentration from the starting monomer concentration. The equilibrium monomer concentration was determined using a sedimentation assay: protein was aggregated for a time corresponding to 3τ (24 h) of the ThT fluorescence-monitored

DOI: 10.1021/acs.biochem.7b00894
Biochemistry 2017, 56, 5931−5942

kinetics and then centrifuged at 70000*g* for 1 h at 25 °C using a TLA100 rotor in a tabletop Beckman Optima Max-XP ultracentrifuge. The protein concentration in the supernatant was then determined by measuring the tryptophan fluorescence at 357 nm, upon excitation at 295 nm.

For determination of the kinetics of monomer loss during aggregation, aliquots of the aggregating protein were withdrawn at different times during fibril formation and subjected to ultracentrifugation at 70000*g* for 1 h. The concentration of protein remaining in the supernatant was that of the monomer remaining in solution.

Seeding Experiments. Fibrils formed by 25 μM moPrP aggregates [aggregates obtained at 3τ (24 h) of the ThT fluorescence-monitored kinetics] were sonicated to prepare the seed. The aggregate suspension was kept on ice and sonicated using a micro probe with the following parameters: amplitude, 30%; pulse, 5 s on and 5 s off; total time, 2 min. For all the seeded reactions, ThT was added to a concentration equal to the protein concentration; 200 μL aliquots of the protein in 1× fibrillization buffer, containing fixed concentrations of seed, were then transferred to different wells of a 96-well plate, which was incubated at 37 °C and shaken at 480 rpm using the Fluoroskan Ascent Microplate Fluorometer. The ThT fluorescence was measured at 475 nm upon excitation at 440 nm. The readings were acquired every 10 min. The final ThT fluorescence varied slightly across seeding experiments, because of problems inherent to sonication; hence, the data were plotted as fractional change plots to compare the seeded to unseeded reactions. An equal volume of seed suspension replaced the volume of the reaction mixture, so that the desired percentage (v/v) of the seed concentration was obtained. The initial rate constant of polymerization was determined as the slope of a linear fit to the initial (5%) part of the aggregation curve monitored using ThT fluorescence.

Atomic Force Microscopy (AFM). Samples (100 μL) from a 50 μM wt moPrP fibrillization reaction mixture were withdrawn at different times, applied to freshly cleaved mica, and incubated for 5 min. After the mica surface had been rinsed five times with doubly filtered Milli-Q water, the samples were dried under vacuum for 1 h, before being scanned. The AFM images were acquired using a Bruker Dimension FastScan Bio AFM instrument (Bruker Inc.) in tapping mode (air). To determine the height and length of the aggregates, the profile option of WSXM software[39] was used.

Data Analysis and Curve Fitting. The kinetic curves measured by monitoring ThT fluorescence were fitted to the equation

$$S = S_0 + \frac{S_\infty - S_0}{1 + e^{-\left(\frac{t - t_{50}}{\tau}\right)}} \tag{1}$$

where S, S_0, and S_∞ are the fluorescence signals at times t, zero, and ∞, respectively, t_{50} is the time at which the change in signal is 50%, and τ is a characteristic time constant. The lag time (t_{lag}) was calculated as $t_{lag} = t_{50} - 2\tau$ as described previously.[40] A similar value for t_{lag} was obtained by determining the time taken to complete 15% of the reaction. The values of S, S_0, and S_∞ were used to calculate the fractional change (F) at each time point:

$$F = \frac{S - S_0}{S_\infty - S_0} \tag{2}$$

The apparent rate constant of elongation was determined by fitting the kinetic data points, after excluding the initial 15% of the aggregation curve, to a single-exponential equation:

$$S = S_0 + a[1 - e^{-\left(\frac{t}{\tau_{el}}\right)}] \tag{3}$$

where a is the amplitude of the signal and τ_{el} is the time constant of elongation.

To check whether the kinetic curves of aggregation determined at different protein concentrations collapse upon phenomenological scaling, the signal changes and times of a kinetic curve were normalized to S_∞ and t_{50}, respectively.

The theory and the equations underlying the linear perturbation analysis of the kinetic data according to a NDP model, with or without augmentation by a secondary pathway, were described previously.[41] A fundamental premise in the analysis is that an equilibrium (defined by equilibrium constant K_{n^*}) is established between the monomer and an oligomeric nucleus (comprised of n^* monomers) and monomer. Only the initial (5%) part of the kinetic curve of aggregation is examined. The concentration of prenuclear oligomers is assumed to be much smaller than the concentrations of both the free monomer, $c(t)$, and the polymerized monomers, $\Delta(t)$. Hence

$$\Delta(t) = c_0 - c(t) \tag{4}$$

where c_0 is the total monomer concentration and $\Delta(t)$ changes upon monomer addition or loss at the polymer ends; this process is assumed to be independent of length for long polymers. Consequently

$$\frac{d\Delta}{dt} = (k_+ c - k_-)c_p \tag{5}$$

where k_+ and k_- are the rate constants of polymerization and depolymerization, respectively, and c_p is the concentration of polymers. k_+ and k_- are related by the critical concentration c_s as $k_- = k_+ c_s$.

The rate of homogeneous polymer formation can be described as

$$\frac{dc_p}{dt} = k_+ c c_{n^*} - k_-^* c_{n^*+1} \tag{6}$$

The polymer size is $n^* + 1$ and larger; k_+ is the rate constant for monomer addition, and k_-^* is the rate constant for dissociation to the nucleus (n^*). Monomer loss from the nucleus does not affect the total concentration of polymer. k_+ is the same for addition of the monomer to both the nucleus and the polymer. Eq 6 then becomes

$$\frac{dc_p}{dt} = k_+ c c_{n^*} = k_+ K_{n^*} c^{n^*+1} \tag{7}$$

The following equation for homogeneous nucleation was used to analyze the kinetic curve of aggregation:

$$\Delta = A[1 - \cos(Bt)] \tag{8}$$

where A describes the apparent shape of the kinetic curve and B is an effective rate constant for nucleation. Only the initial 5% of the kinetic data was used because of the oscillatory behavior of the cos function. A plot of $\log\{(B^2A)/[c_0(c_0 - c_s)]\}$ versus $\log c_0$ gives n^*:

$$\log \frac{B^2 A}{c_0(c_0 - c_s)} = \log k_+^2 K_{n^*} + n^* \log c_0 \tag{9}$$

DOI: 10.1021/acs.biochem.7b00894
Biochemistry 2017, 56, 5931−5942

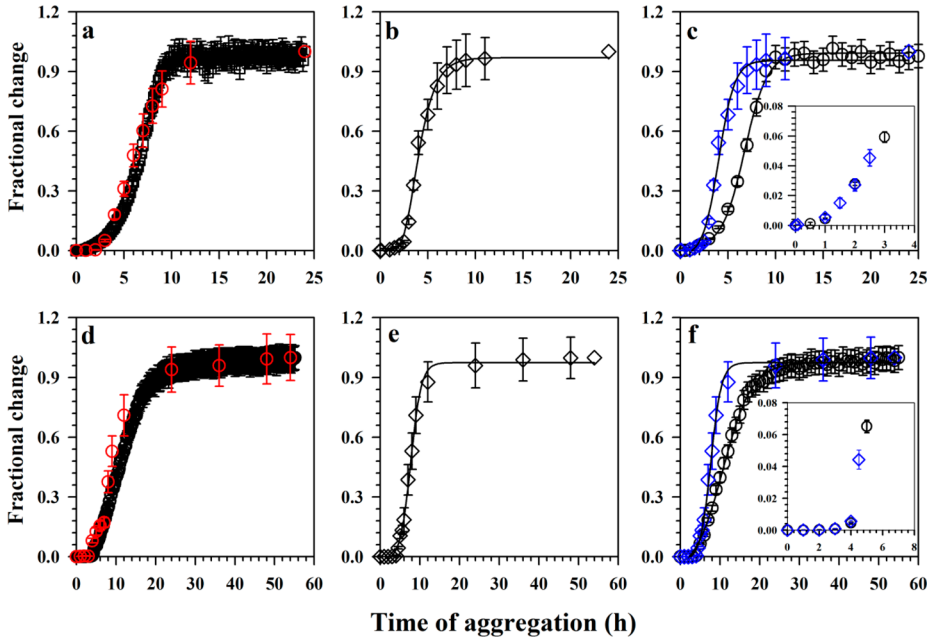

Figure 1. Amyloid fibril formation by moPrP at pH 7.4 and 37 °C. Panels a–c show data for wt moPrP, and panels d–f show data for G126V moPrP. The aggregation of 50 μM wt (a) and G126V moPrP (d) was monitored by measurement of ThT fluorescence, both by using the Fluoroskan Ascent Microplate Fluorometer (with pre-added 50 μM ThT) (black circles) and by using a Fluorolog-3 Spectrofluorometer (without any pre-added ThT) (red circles). The aggregation of 50 μM wt (b) and G126V moPrP (e) was monitored directly by measurement of the fraction of total protein in the aggregates (see Materials and Methods). The fractional progress of the reaction is plotted in panels c and f, where the data from panels a and b and panels d and e, respectively, have been normalized between values of 0 and 1 using eq 2: Fluoroskan ThT fluorescence (black circles) and fibril concentration (blue diamonds). The insets in panels c and f show the initial 5% of the reactions. In panels a–f, the lines through the data are nonlinear least-squares fits to eq 1 and the error bars are the standard deviations from three independent experiments using at least two different preparations of protein.

The value of c_s was found to be 4.0 μM for wt moPrP and 13 μM for G126V moPrP (see the Results and Discussion).

It is possible that the rate of polymerization is accelerated by secondary nucleation in addition to homogeneous nucleation. Secondary nucleation processes may occur by either fragmentation, branching, or heterogeneous nucleation. In each case, the rate is proportional to the concentration of polymerized monomers $[\Delta(t)]$. The three processes can be described by a general parameter, Q. Thus

$$\frac{dc_p}{dt} = k_+K_{n^*}c^{n^*+1} + Q(c_0 - c) \quad (10)$$

For the initial 2–5% of the data, eq 10 can be solved by the linear perturbation approach to yield the following solution:

$$\Delta = A[\cosh(Bt) - 1] \quad (11)$$

where A directs the apparent shape of the kinetic curve and B is an effective rate constant for initial fibril growth. For the secondary process, Q affects the values of both parameters A and B. However, the product of these two parameters, B^2A, remains unaffected by the secondary process, and it is then still possible to derive the nucleus size using eq 10 without any specification of parameter Q.

Parameters A, B, n^*, c_0, and c_s were used to determine the value of k_+Q_0 at each initial monomer concentration (c_0), by using eq 12.

$$k_+Q_0 = \frac{B^2 + (n^* + 1)\left(\frac{B^2A}{c_0}\right)}{c_0 - c_s} \quad (12)$$

The type of secondary process can be deduced from the dependence of $\log(k_+Q_0)$ on $\log(c_0)$. In the case of fragmentation, the slope of the plot will be 0; for lateral growth, the slope will be 1, and for heterogeneous nucleation, the slope will give the heterogeneous nucleus size.

All fits were performed using Levenberg–Marquardt algorithm in SigmaPlot 12.

RESULTS AND DISCUSSION

Amyloid Fibril Formation by Mouse Prion Protein. Previous studies of amyloid fibril formation by recombinant prion protein had shown that at physiological pH, and in the presence of chemical denaturants, the prion protein misfolds and aggregates into long straight amyloid fibrils,[13,16] but the mechanism of amyloid fibril formation was not established. This study characterizes in quantitative detail the mechanism of amyloid fibril formation by the full-length mouse prion protein (moPrP), at pH 7.4 and 37 °C, in the presence of 2 M guanidine hydrochloride (GdnHCl), with agitation. Additionally, the effect of the protective mutation, G126V, on the structure, stability, and aggregation of moPrP was also characterized (Figure S1 and Figure 1).

The far-UV CD spectra of wt and G126V moPrP were found to be very similar at pH 7.4 (Figure S1a). A GdnHCl-induced equilibrium unfolding study indicated that G126V and wt moPrP had similar stabilities (Figure S1b). Hence, it appears that, similar to several other pathogenic mutations in the unstructured NTR, the G126V mutation did not affect the global stability of moPrP.[38,42,43] Thermodynamic stability is known to be a major modulator of the misfolding and aggregation propensities of the prion protein,[35,36,43] but not

DOI: 10.1021/acs.biochem.7b00894
Biochemistry 2017, 56, 5931–5942

always.[35,42] It became important to study whether the G126V mutation had an effect on amyloid fibril formation, despite it not affecting the structure and stability of the protein.

The kinetics of amyloid fibril formation by wt and G126V moPrP were conveniently studied by performing the reactions in the presence of ThT, for continuous monitoring of the progress of the fibril formation reaction.[44] The kinetics was also studied in the absence of ThT, to probe the effects of pre-added ThT on the fibril formation reaction (Figure 1). The kinetic curves determined in these two ways were coincident, which suggested that the fibril formation reactions are not affected by the pre-addition of ThT (Figure 1a,d). When monitored using ThT fluorescence, the kinetics of amyloid fibril formation was found to be sigmoidal in nature (Figure 1). When the amount of soluble monomer present at any time during the aggregation reaction was measured using the sedimentation assay, similar sigmoidal kinetics was observed (Figure 1b,e). The kinetic curves of aggregation monitored by the ThT fluorescence and sedimentation assays overlapped in the initial phase (Figure 1c,f). However, the overall kinetics as monitored by the sedimentation assay appeared to be faster than that measured by ThT fluorescence. The apparent difference in the kinetics measured by these two probes of aggregation could be because (1) oligomers may have formed in the early phase of aggregation, which did not bind to ThT to the same extent that amyloid fibrils did,[25] or (2) the association of monomers into fibrils preceded conformational conversion.[16,45] It should also be noted that the kinetic curves obtained using each probe were highly reproducible, as reflected in the small errors of measurement (Figure 1). Such highly reproducible kinetic curves are important for quantitatively analyzing the amyloid fibril formation reaction.

A Single Mechanism Explains the Kinetics of PrP Fibril Formation at Different Protein Concentrations. The kinetics of amyloid fibril formation was studied for wt and G126V moPrP, across protein concentrations ranging from 10 to 100 μM (Figure S2). The aggregation kinetics remained sigmoidal at all protein concentrations (Figure S2a,c). Upon phenomenological scaling, the kinetic curves obtained at different protein concentrations for wt moPrP as well as for G126V moPrP were found to collapse into a single kinetic curve (Figure S2b,d) (see Materials and Methods).[46] Hence, the mechanisms that describe the aggregation of wt moPrP, as well as of G126V moPrP, are the same for each protein variant, over the range of protein concentrations studied.

The aggregation kinetics of G126V moPrP was significantly different from that of wt moPrP in the duration of the lag phase (t_{lag}) and the time taken to complete 50% of the reaction (t_{50}). These differences in the kinetics of wt and G126V moPrP, which were more evident in a plot of fractional change versus log time (Figure S2b,d), suggest that these two proteins might aggregate differently. It should be noted that for G126V moPrP, phenomenological scaling was done for only protein concentrations in the range of 30−100 μM, because there was no significant ThT fluorescence detected for protein concentrations of ≤20 μM. This result indicated that the critical concentration for G126V moPrP fibril formation might be significantly higher than that for wt moPrP fibril formation.

PrP Fibril Formation Can Be Described by a NDP Mechanism. The amyloid fibril formation reactions of wt and G126V moPrP showed sigmoidal kinetics with distinct lag, elongation, and saturation phases, typical of a fibril formation reaction that occurs via a NDP mechanism. However, such kinetics may also be observed when polymerization is isodesmic.[47−49] To establish the mechanism, the dependence of the apparent rate constant of fibril elongation, as well as the final amplitude of the fibril formation reaction, on protein concentration was measured (Figure 2a,b). The apparent rate constant of fibril elongation measured by ThT fluorescence was not dependent on protein concentration, whereas the relative final amplitude of the ThT fluorescence increased linearly with an increase in protein concentration. From the intercepts on the x-axis of the straight-line fits to both the final ThT fluorescence amplitude and the fraction of total protein in fibrils, the critical concentrations were found to be ∼3.5 and ∼9.5 μM for wt and G126V moPrP, respectively (Figure 2b).

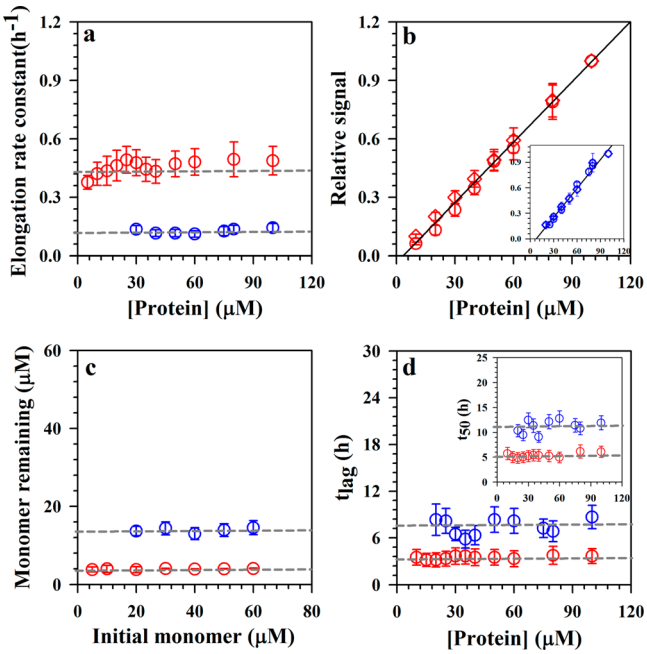

Figure 2. Dependence of aggregation kinetics on moPrP concentration. The kinetics of the fibril formation reaction was monitored by measurement of ThT fluorescence. Panel a shows the dependence of the elongation rate constant on wt moPrP (red circles) and G126V moPrP (blue circles) concentration. Panel b shows the dependence of the final amplitude monitored by ThT fluorescence (red circles) and by measurement of the fraction of the total protein in aggregates (red diamonds) on the concentration of wt moPrP. The inset in panel b shows the dependence of the final amplitude monitored by ThT fluorescence (blue circles) and by direct measurement of the fraction of the total protein in aggregates (blue diamonds) on the concentration of G126V moPrP. In panel b, the linear fit through the data extrapolates to intercept the x-axis at the critical concentration of 3.5 μM. In the inset of panel b, the linear fit through the data extrapolates to intercept the x-axis at the critical concentration of 9.5 μM. Panel c shows a plot of the final concentration of the monomer remaining in the aggregation reaction mixture vs the initial monomer concentration of wt (red circles) and G126V (blue circles) moPrP (see Materials and Methods). Panel d shows the dependences of t_{lag} (lag time) on wt moPrP (red circles) and G126V moPrP (blue circles) concentration. The inset of panel d shows the dependence of t_{50} on wt moPrP (red circles) and G126V moPrP (blue circles) concentration. In all three panels, the short dashed lines are drawn through the data to guide the eye and are not fits. Error bars denote the standard deviations determined from three independent experiments that utilized at least two different preparations of protein.

DOI: 10.1021/acs.biochem.7b00894
Biochemistry 2017, 56, 5931−5942

If indeed there exists a critical concentration for each protein variant below which it does not aggregate, then it was expected that when fibrils were fully formed, they should be present in equilibrium with monomer, with the monomer concentration being equal to the critical concentration. The final monomer concentrations present at equilibrium when aggregation was performed at different concentrations of wt and G126V moPrP were found to be ~4 and ~13 μM, respectively (Figure 2c). Furthermore, no amyloid fibril formation was detected over a period of 72 h, when the fibril formation reactions for wt and G126V moPrP were performed at 4 and 15 μM, respectively (data not shown). These two observations confirmed that a critical concentration exists for moPrP fibril formation and that the critical concentration for G126V moPrP is higher than that of wt moPrP. Similar differences in the critical concentration for $A\beta_{1-40}$ and $A\beta_{1-42}$ aggregation had been shown to delay misfolding and aggregation[50] and thus might increase the age of onset and delay the progression of pathological effects.[51]

For aggregation via a NDP mechanism, the lag time and t_{50} might be expected to have strong dependencies on protein concentration. However, both the lag time and t_{50} were found to vary only marginally with protein concentration (Figure 2d). The logarithm of the lag time (or of t_{50}) had a very weak and positive linear dependence on the logarithm of protein concentration (Figure S3). A very weak dependence is consistent with a monomeric nucleus,[29,52] but the positive dependence was surprising. One possible explanation is that the NDP pathway leading to the formation of fibrils competes with an off-pathway aggregation reaction, such as the formation of off-pathway oligomers. In fact, an analytical solution of the equations describing such competing aggregation reactions predicts such a positive dependence.[53]

Off-Pathway Oligomers Form Transiently during the Fibril Formation Reaction of moPrP. The observation that the kinetics of fibril formation appeared to be marginally faster when monitored by the sedimentation assay than when measured by ThT fluorescence was the first indication that the fibril formation reaction may be accompanied by transient oligomer formation. In AFM images of aggregating protein samples of wt and G126V moPrP collected at different time points (Figure 3 and Figure S4), no oligomers were observed during the first 15 min of aggregation of wt moPrP: the mica surface coated with the aggregation sample could not be distinguished from the mica surface coated with an equimolar amount of monomer (Figure 3). After 15 min, and ≤2 h, which was the end of the lag phase, only spherical oligomers were observed and no fibrils were detected by AFM. After 4 h, oligomers were not detected. Fibrils were observed from 4 h. At 7 h, individual fibrils were mostly seen, and not clumps. At 10 h, when fibril formation was nearly complete, the fibrils were found to occur in clumps and had a length in the range of 800–1500 nm. The fibril height was 8.3 ± 1.2 nm, as determined from Gaussian fits to the distributions of their measured heights (data not shown).

Similarly, oligomers could not be detected during the first 15 min of aggregation of G126V moPrP (Figure S4). After 15 min, and ≤7 h, which was the end of the lag phase, spherical oligomers but not fibrils were observed by AFM. At 10 h, oligomers were not detected, and only very few fibrils were observed. Toward the end of the fibril formation reaction, at 20 h, only fibrils were observed, and these fibrils were found to occur in clumps and have a length and height that were very similar to those of wt moPrP (data not shown). AFM images

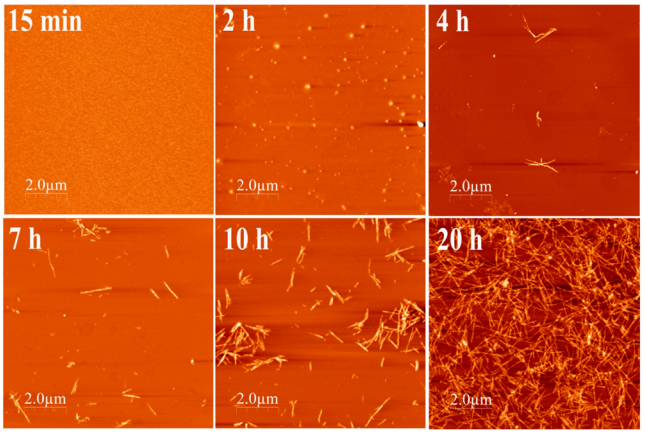

Figure 3. Structural characterization of the progress of the amyloid fibril formation reaction. AFM images were obtained at 15 min, 2 h, 4 h, 7 h, 10 h, and at 20 h during the aggregation of 50 μM wt moPrP. The images are all shown in topography mode. The height of the oligomers seen at 15 min was 2.4 ± 0.4 nm, and the height of the fibrils seen at longer times was 8.3 ± 1.2 nm.

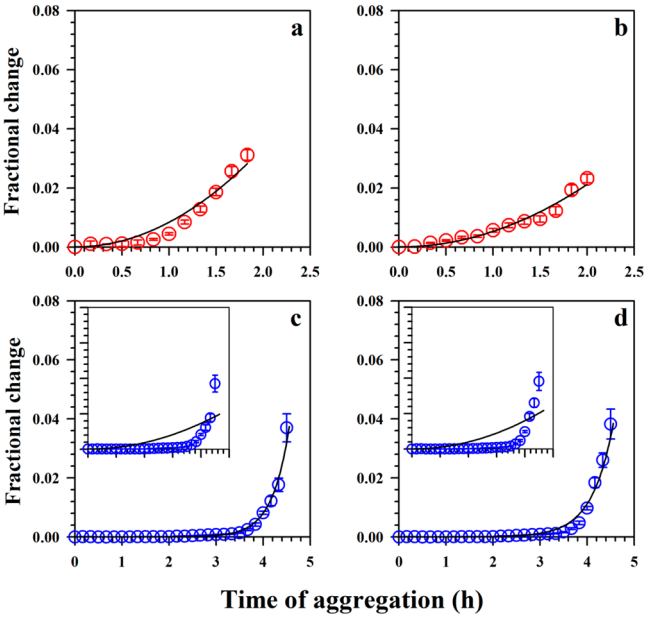

Figure 4. Initial progress of the amyloid fibril formation reactions. Panels a–d show the initial parts of the kinetic curves of aggregation, monitored by ThT fluorescence, of 30 μM (a and c) and 60 μM (b and d) wt moPrP (red circles) and G126V moPrP (blue circles). In panels a and b, the black lines are least-squares fits to eq 8. In panels c and d, the black solid lines are least-squares fits to eq 11. The insets in panels c and d show the same data fit to eq 8 (see Materials and Methods). Error bars represent the standard deviations determined from three independent experiments that utilized at least two different preparations of protein.

showed that both the oligomers and final fibrils formed by wt and G126V moPrP had similar morphologies. After aggregation of wt moPrP for 4 h, and after 7 h in the case of G126V moPrP, fibrils were found to grow progressively in size. It appears that growth occurred by addition of monomer; no oligomers were seen after these times (Figure 3 and Figure S4). The AFM images showed that oligomers formed early during the aggregation reaction and disappeared before fibril formation could be detected, indicating that the oligomers did not form

DOI: 10.1021/acs.biochem.7b00894
Biochemistry 2017, 56, 5931–5942

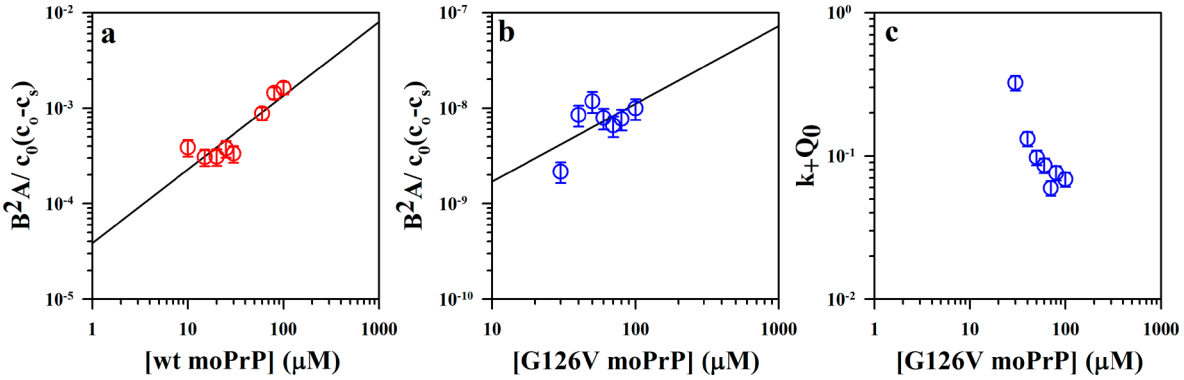

Figure 5. Determination of the size of the nucleus as well as the nature of the secondary pathway for fibrillization. Panel a shows data for wt moPrP, and panels b and c show data for G126V moPrP. The quantities $(B^2A)/[c_0(c_0 - c_s)]$ and k_+Q_0 were determined at each protein concentration from data such as those shown in Figure 4, as described in Materials and Methods. The straight lines through the data in panels a and b are least-squares fits. The slope of the plot yields the nucleus size and was 0.77 ± 0.13 and 0.80 ± 0.14 for wt and G126V moPrP, respectively. The values of k_+Q_0 at different concentrations of G126V moPrP (c) were calculated using the parameters described in Materials and Methods. Error bars represent the spread in the data determined from two or more independent experiments that utilized at least two different preparations of protein.

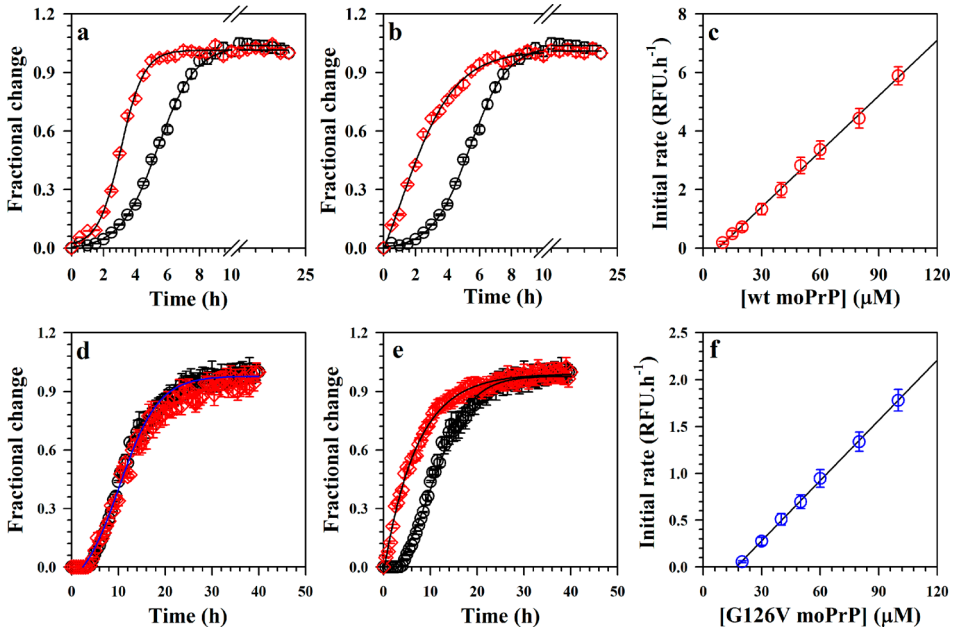

Figure 6. Effect of seeding on the kinetics of moPrP aggregation. The ThT fluorescence-monitored kinetics of amyloid fibril formation by 20 μM wt moPrP in the presence of (a) 1% and (b) 10% sonicated seed (red diamonds) and in the absence of seed (black circles) are shown. Similarly, amyloid fibril formation by 20 μM G126V moPrP in the absence of seed (black circles) and in the presence of (d) 1% and (e) 10% sonicated seed (blue diamonds) is shown. Panels c and f show the dependence of the initial rate of the reaction on initial wt and G126V moPrP concentration in the presence of 10% sonicated seeds. When extrapolated to intersect the x-axis, the linear fits through the data yield critical concentrations of 3.6 and 13.6 μM for wt and G126V moPrP, respectively. The lines through the data in panels a and d are least-squares fits to eq 1. The solid lines through the data in panels b and e are least-squares fits to eq 1 (for unseeded reactions) or eq 3 (for seeded reactions). In each panel, the error bars represent the spread in the data determined from two or more independent experiments, which utilized at least two different preparations of protein.

on the direct pathway of fibril formation. Unfortunately, the observation that transient off-pathway oligomers were present during the course of fibril formation by wt and G126V moPrP precluded the use of AmyloFit, an elegant tool for the global analysis of kinetic data on aggregation via NDP occurring in the absence of off-pathway oligomer formation,[54] which could have provided detailed information about the aggregation reactions.

Fortunately, the oligomers were found to be populated to only an insignificant extent during the initial 5% phase of fibril formation: the kinetics of monomer loss (Figure S5) suggests that the fraction of monomer present in the oligomers in the initial 5% phase of fibril formation is insignificant as compared to the fraction of monomer present in the fibrils (Figure 1). This meant that the initial phase could be used to perform linear perturbation analysis,[41,55] which provides information about the size of the nucleus and whether nucleation is homogeneous or whether secondary nucleation processes are operative.

Quantitative Analysis of the Early Phase of PrP Fibril Formation. The linear perturbation method was used to examine the initial phase of fibril formation. This mathematical method predicts that for homogeneous nucleation, the initial part of the kinetic curve of aggregation should be able top be described by either a t^2 or a cos t function.[41,55] The initial 5% of

DOI: 10.1021/acs.biochem.7b00894
Biochemistry 2017, 56, 5931−5942

the kinetics of wt moPrP aggregation fit reasonably well to a cos t function (Figure 4a,b) (eq 8). A t^2 function fit equally well (fit not shown). Thus, the values of parameters A and B in eq 8 could be determined at each protein concentration. The size of the homogeneous nucleus, n^* (Figure 5a), was then determined by the use of eq 9, which was derived from the perturbation analysis. The equilibrium nucleus size, n^*, of wt moPrP was determined to be 1.

Analysis of the kinetic data of G126V moPrP aggregation indicated that the aggregation mechanism was more complex than that of wt moPrP: the initial parts of the kinetic curves of fibril formation could not be described by a cos t (or t^2) function; instead, a cosh t function (eq 11) was required to fit the data (Figure 4c,d). A cosh t dependence is evidence of secondary processes being operative. The kinetic data were analyzed further taking into account that secondary processes were operative. The values of A and B (eq 11) were determined at each protein concentration and were then used (eq 9) to determine the size of the equilibrium nucleus. As in the case of wt moPrP, a value of 1 was obtained for the equilibrium nucleus size, n^*, of G126V moPrP (Figure 5b). It is to be noted that the quantity B^2A in eq 9 has the same form, regardless of whether secondary processes are operative.[55] Thus, the size of the equilibrium homogeneous nucleus can be determined even when a secondary nucleation pathway is operative.

Hence, it appears that for both wt and G126V moPrP, fibril formation proceeds via a monomeric nucleus. A previous study of the aggregation of huntingtin had shown that the nucleus was a monomer, and it was proposed that nucleation corresponded to conformational conversion within the monomer.[52] In the study presented here, the nucleus was considered to be the least stable species on the aggregation pathway.[41,53,56] Although both the variants of moPrP form fibrils via a monomeric nucleus, initial fibril growth is slower in the case of G126V moPrP, which is evident from the delayed lag phase (Figures 2d and 4).

A monomeric nucleus for the aggregation of proteins, leading to neurodegenerative disease, is certainly not improbable. When the disease-related protein is intrinsically disordered, aggregation could start after a partially folded intermediate misfolds to form a monomeric nucleus; when it is a folded protein, aggregation could start after a partially unfolded intermediate misfolds to form a monomeric nucleus.[57] It is perhaps not surprising that several disease-linked multimeric proteins have to dissociate into monomers before misfolding can occur.[58,59] A misfolded monomeric nucleus is consistent with two possible aggregation mechanisms. In one mechanism, spontaneous aggregation occurs upon the productive interaction between misfolded and native monomers.[28,52] The second mechanism requires a productive association between two misfolded monomers.[60] In the case of G126V moPrP, the decreased nucleation rate, and increased lag time, might be due to altered interactions between the misfolded monomer and a native monomer, or between two misfolded monomers.

The linear perturbation method was then used to determine the nature of the secondary processes that operate during the fibril formation reaction of G126V moPrP. The values obtained for parameters A and B at different starting monomer concentrations were used to determine the quantity k_+Q_0 at each protein concentration (see Materials and Methods). The type of secondary process could then be determined from the slope of a log–log plot of k_+Q_0 versus starting monomer concentration (Figure 5c). A slope of 0 is indicative of the major secondary process being fragmentation, and when the slope is 1, the major secondary process is lateral growth. A slope value of >1 is indicative that the secondary process is heterogeneous nucleation; then the value of the slope provides the heterogeneous nucleus size. The dependence of the quantity k_+Q_0 on protein concentration suggests that for G126V moPrP, the main secondary nucleation pathway is heterogeneous nucleation (Figure 5c). It is, however, very difficult to rule out the possibility that fragmentation and branching do not occur.

PrP Fibril Growth Occurs by Monomer Addition. An important test for the NDP mechanism is whether the lag phase can be eliminated by adding preformed fibrils (seeds). The addition of 1 wt % seed partially abolished the lag phase seen for fibril formation with 25 μM wt moPrP, whereas the addition of 2 and 10 wt % seed completely abolished the lag phase (Figures 6 and 7). Similarly, the addition of 1% G126V seed did not abolish the lag phase seen for fibril formation with 25 μM G126V, whereas the addition of 10% G126V seed resulted in complete abolition of the lag phase (Figure 6d,e). At a seed concentration of 10 wt %, the initial rate of aggregation was found to be dependent linearly on monomer concentration, for both wt moPrP (Figure 6c) and G126V moPrP (Figure 6f),

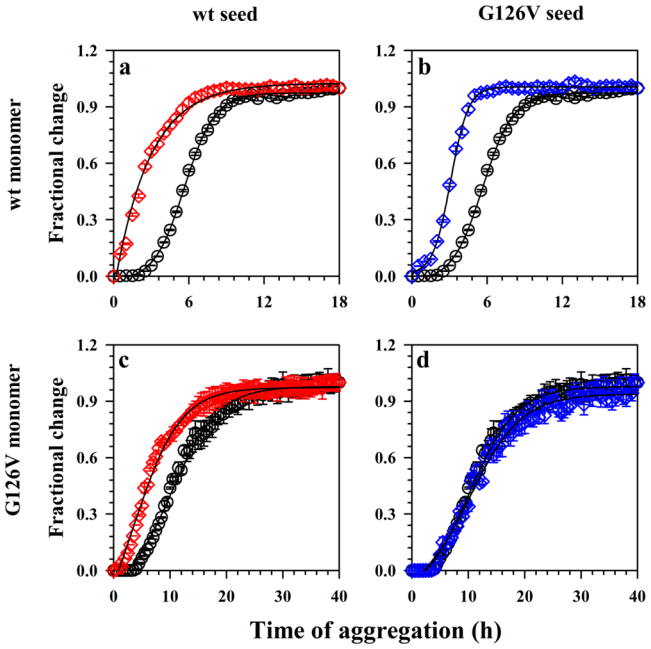

Figure 7. Effect of cross-seeding on the kinetics of aggregation of moPrP. In panels a and b are shown the ThT fluorescence-monitored kinetics of amyloid fibril formation by 25 μM wt moPrP in the absence of seed (black circles) and in the presence of 2% wt moPrP (red diamonds) and G126V moPrP (blue diamonds) sonicated seeds, respectively (see Materials and Methods). In panels c and d are shown the ThT fluorescence-monitored kinetics of amyloid fibril formation by 25 μM G126V moPrP in the absence of seed (black circles) and in the presence of 2% wt moPrP (red diamonds) and G126V moPrP (blue diamonds) sonicated seeds, respectively. In panel a, the solid lines through the data are least-squares fits to eq 1 (for unseeded reactions) or eq 3 (for seeded reactions). In panels b–d, the solid lines through the data are least-squares fits to eq 1. In each panel, the error bars represent the spread in the data determined from two or more independent experiments using at least two different preparations of protein.

DOI: 10.1021/acs.biochem.7b00894
Biochemistry 2017, 56, 5931–5942

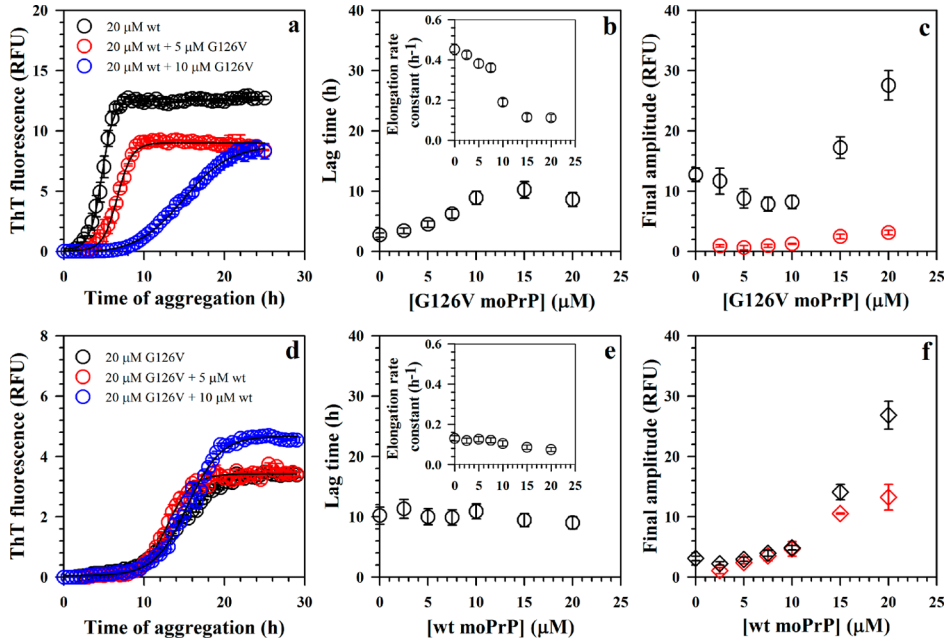

Figure 8. Effect of the presence of G126V moPrP on amyloid fibril formation by wt moPrP. The aggregation of 20 μM wt moPrP (a) and 20 μM G126V moPrP (d) in the presence different concentrations of G126V moPrP and wt moPrP, respectively, was monitored by the ThT fluorescence assay. Panels b and e show the lag times, and elongation rate constants (insets), of 20 μM wt moPrP and 20 μM G126V moPrP, respectively, in the presence of different concentrations of G126V and wt moPrP, respectively. Panels c and f show the final amplitudes of amyloid fibril formation by 20 μM wt moPrP (black circles) and 20 μM G126V moPrP (black diamonds) in the presence of different concentrations of G126V and wt moPrP, respectively, and the final amplitudes of amyloid fibril formation by different concentrations of G126V moPrP (red circles) and wt moPrP (red diamonds). The solid lines through the data in panels a and d are nonlinear least-squares fits to eq 1. In each panel, the error bars represent the standard deviations determined from three independent experiments that utilized more than two different preparations of protein.

suggesting that monomeric protein adds directly to the seed during fibril growth. The linear dependence also confirms the assumption made in the linear perturbation analysis,[41,55] that fibril growth occurs by monomer addition. A recent study with recombinant full-length PrP also reported such linear dependence at lower protein concentrations, although saturation was observed at higher protein concentrations.[61] However, the aggregation conditions used in that study were significantly different from those used in the study presented here. Such a linear dependence had also been observed previously for the aggregation of the yeast prion protein, and in that case, too, it had been concluded that fibril growth occurred by monomer addition.[62]. Nevertheless, the possibility that a very low concentration of the aggregation-competent oligomer exists in a pre-equilibrium with monomer, which adds to the growing fibrils, cannot be easily ruled out.

Cross-Seeding Experiments Reveal That the G126V Mutation Decreases the Seeding Efficiency. A previous study using transgenic mice had shown that the G126V mutant variant was resistant to prion conversion and was capable of preventing the propagation of wt prions in a dose-dependent manner.[11] However, the mechanism behind the protective nature of the G126V mutation has remained unclear. To test this phenomenon under *in vitro* conditions, seeding experiments were conducted with sonicated fibrils (seeds) and monomers of wt and G126V moPrP (Figure 7). The addition of 2 wt % seed to 25 μM wt monomer completely abolished the lag phase (Figure 7a), whereas the addition of 2 wt % seed to 25 μM G126V monomer only partially abolished the lag phase (Figure 7c). Similarly, the addition of 2% G126V seed to 25 μM wt monomer partially abolished the lag phase (Figure 7b), whereas the addition of 2% G126V seed to 25 μM G126V monomer did not affect the lag phase at all (Figure 7d). Hence, the G126V mutation weakened the ability of wt seed to interact with G126V monomer and of G126V seed to interact with both wt and G126V monomers. These observations suggest that residue position 126 is important in both the seed and monomer, for additionof monomer to seed. The mutation appears to directly affect the affinity of seed for monomer. *In vivo*, if the binding affinity of infectious seed for monomer were to be sufficiently decreased by the G126V mutation, then given the low concentration of monomer present in and on the cell, it is possible that binding and, hence, conformational conversion cannot occur.

The G126V Mutant Variant Affects the Kinetic Parameters of wt moPrP Aggregation. Patients carrying the G126V mutation are expected to express both wt and mutant variants of the prion protein.[4,11] Hence, it is important to characterize the effect of the presence of the G126V mutant variant on the aggregation kinetics of wt moPrP. When 20 μM wt moPrP was aggregated in the presence of G126V moPrP at concentrations below the critical concentration for fibril formation by G126V moPrP, the lag time became longer, elongation became slower, and there was less fibril formation (Figure 8a–c). In contrast, when 20 μM G126V moPrP was aggregated in the presence of wt moPrP, the lag time, elongation rate constant, and extent of fibril formation were not affected (Figure 8d–f). Hence, the presence of the protective mutant variant, G126V moPrP, inhibits nucleation and elongation during wt moPrP aggregation.

It is known that the association of PrP^C molecules via the middle hydrophobic region, where the G126V mutation is present, is an important step that initiates PrP^{Sc} formation.[6,63] Importantly, the rate-determining step in both oligomeriza-

DOI: 10.1021/acs.biochem.7b00894
Biochemistry 2017, 56, 5931–5942

tion,[42,64] and amyloid fibril formation by PrP,[65] has been shown to be dimer formation. A study with huPrP mutant variants that contains amino acid substitutions at residue position 128 has also shown that this region is important for dimer formation, and the commencement of amyloid fibril formation.[66] Our study shows that the protective mutation in the middle hydrophobic region decreases not only the level of initial interaction between two monomeric PrP molecules, regardless of whether both the monomeric proteins are wt moPrP or G126V moPrP, or whether one is wt moPrP and the other is G126V moPrP, but also the level of interaction between fibril and monomer, regardless of whether the fibril is aggregated wt moPrP or G126V moPrP or whether the monomer is wt moPrP or G126V moPrP.

Physiological Relevance of the Existence of a NDP Mechanism for moPrP Fibrillization. Studies with different amyloidogenic proteins have suggested that the NDP mechanism might be a good description of amyloid-mediated cell death.[27,67−69] A study of the aggregation of a polyQ sequence suggested that the nucleation rate constant may determine the age of onset of Huntington's disease.[52] Moreover, it has been shown for polyQ peptides that nucleation suffices to initiate neuronal loss in certain brain regions.[70,71] In the study presented here, it has been shown that prion protein aggregation occurs by a NDP mechanism. The concentration of the prion protein on and in cells is not known but is likely to be very low.

A salient feature of an amyloid fibril formation reaction that can be describedas NDP is that a critical concentration exists below which fibril formation, whether seeded or unseeded, cannot occur. The observation that the critical concentrations for the formation of fibrils by wt moPrP and G126V moPrP are ∼4 and ∼13 μM, respectively, indicates that G126V moPrP will not form fibrils at concentrations below 13 μM, while wt moPrP will not form fibrils only at concentrations below 4 μM. The critical concentration in a NDP mechanism is a gauge of the binding constant for addition of monomer to fibril,[72] and hence, the study presented here has shown that the binding of mutant monomer to mutant fibril is weaker than that of wt monomer to wt fibrils (see above). It is likely that in the crowded environment inside the cell as well as on the cell surface, the critical concentrations are lower, but it is very unlikely that the critical concentration for amyloid fibril formation by G126V moPrP will not remain 3−5-fold higher than that for fibril formation by wt moPrP. Thus, a simple explanation for the equivalent G127V mutation in huPrP being protective in humans is that it increases the critical concentration to a level above the concentration to which the protein is expressed in and on cells, so that fibril formation will not occur even upon infection with wt moPrP fibrils.

CONCLUSION

In summary, this study shows that both wt and G126V moPrP form amyloid fibrils via a NDP mechanism. All the characteristic criteria for a NDP reaction are met. wt moPrP aggregates predominantly via a homogeneous nucleation pathway with a monomeric nucleus. In the case of G126V moPrP, a secondary nucleation pathway also operates during fibril growth, which seems to be heterogeneous nucleation. A monomeric nucleus for fibril formation suggests that the main nucleating event is conformational conversion within the monomer. Seeding, cross-seeding, and co-aggregation experiments with wt and G126V moPrP seed suggest that the G126V mutation modulates monomer−monomer and monomer−fibril interactions and that the mutant variant has a diminished capacity to add to existing fibril ends. The observation that the mutation increases the critical concentration suggests a simple reason for why it is a protective mutation: it increases the critical concentration to a value higher than the concentration of the prion protein present inside and on cells.

ASSOCIATED CONTENT

Supporting Information

The Supporting Information is available free of charge on the ACS Publications website at DOI: 10.1021/acs.biochem.7b00894.

Figures S1−S5 (PDF)

AUTHOR INFORMATION

Corresponding Author

*National Centre for Biological Sciences, Tata Institute of Fundamental Research, Bengaluru 560065, India. E-mail: jayant@ncbs.res.in. Phone: +91-80-6717-6150.

ORCID

Ambadi Thody Sabareesan: 0000-0003-1418-3410

Jayant B. Udgaonkar: 0000-0002-7005-224X

Funding

J.B.U. is a recipient of a J. C. Bose National Fellowship from the Government of India. This work was funded by the Department of Biotechnology, Government of India, and by the Tata Institute of Fundamental Research.

Notes

The authors declare no competing financial interest.

ACKNOWLEDGMENTS

We thank members of our laboratory for discussion. The AFM images were collected at the Central Imaging and Flow Facility of the National Centre for Biological Sciences.

REFERENCES

(1) Prusiner, S. B. (1982) Novel proteinaceous infectious particles cause scrapie. *Science 216*, 136−144.

(2) Zahn, R., Liu, A., Luhrs, T., Riek, R., von Schroetter, C., Lopez Garcia, F., Billeter, M., Calzolai, L., Wider, G., and Wuthrich, K. (2000) NMR solution structure of the human prion protein. *Proc. Natl. Acad. Sci. U. S. A. 97*, 145−150.

(3) Collinge, J. (2001) Prion diseases of humans and animals: their causes and molecular basis. *Annu. Rev. Neurosci. 24*, 519−550.

(4) Mead, S. (2006) Prion disease genetics. *Eur. J. Hum. Genet. 14*, 273−281.

(5) Peretz, D., Williamson, R. A., Matsunaga, Y., Serban, H., Pinilla, C., Bastidas, R. B., Rozenshteyn, R., James, T. L., Houghten, R. A., Cohen, F. E., Prusiner, S. B., and Burton, D. R. (1997) A conformational transition at the N terminus of the prion protein features in formation of the scrapie isoform,. *J. Mol. Biol. 273*, 614−622.

(6) Norstrom, E. M., and Mastrianni, J. A. (2005) The AGAAAAGA palindrome in PrP is required to generate a productive PrPSc-PrPC complex that leads to prion propagation,. *J. Biol. Chem. 280*, 27236−27243.

(7) Jobling, M. F., Stewart, L. R., White, A. R., McLean, C., Friedhuber, A., Maher, F., Beyreuther, K., Masters, C. L., Barrow, C. J., Collins, S. J., and Cappai, R. (1999) The Hydrophobic Core Sequence Modulates the Neurotoxic and Secondary Structure Properties of the Prion Peptide 106−126,. *J. Neurochem. 73*, 1557−1565.

DOI: 10.1021/acs.biochem.7b00894
Biochemistry 2017, 56, 5931−5942

(8) Abskharon, R. N., Giachin, G., Wohlkonig, A., Soror, S. H., Pardon, E., Legname, G., and Steyaert, J. (2014) Probing the N-terminal β-sheet conversion in the crystal structure of the human prion protein bound to a nanobody. *J. Am. Chem. Soc. 136*, 937−944.
(9) Hum Lim, K., Nguyen, T. N., Damo, S. M., Mazur, T., Ball, H. L., Prusiner, S. B., Pines, A., and Wemmer, D. E. (2006) Solid-state NMR structural studies of the fibril form of a mutant mouse prion peptide PrP 89−143 (P101L). *Solid State Nucl. Magn. Reson. 29*, 183−190.
(10) Mead, S., Whitfield, J., Poulter, M., Shah, P., Uphill, J., Campbell, T., Al-Dujaily, H., Hummerich, H., Beck, J., Mein, C. A., Verzilli, C., Whittaker, J., Alpers, M., and Collinge, J. (2009) A novel protective prion protein variant that colocalizes with kuru exposure. *N. Engl. J. Med. 361*, 2056−2065.
(11) Asante, E. A., Smidak, M., Grimshaw, A., Houghton, R., Tomlinson, A., Jeelani, A., Jakubcova, T., Hamdan, S., Richard-Londt, A., Linehan, J. M., Brandner, S., Alpers, M., Whitfield, J., Mead, S., Wadsworth, J. D. F., and Collinge, J. (2015) A naturally occurring variant of the human prion protein completely prevents prion disease,. *Nature 522*, 478−481.
(12) Zhou, S., Shi, D., Liu, X., Liu, H., and Yao, X. (2016) Protective V127 prion variant prevents prion disease by interrupting the formation of dimer and fibril from molecular dynamics simulations. *Sci. Rep. 6*, 21804.
(13) Bocharova, O. V., Breydo, L., Parfenov, A. S., Salnikov, V. V., and Baskakov, I. V. (2005) In vitro conversion of full-length mammalian prion protein produces amyloid form with physical properties of PrP Sc. *J. Mol. Biol. 346*, 645−659.
(14) Jones, E. M., and Surewicz, W. K. (2005) Fibril conformation as the basis of species-and strain-dependent seeding specificity of mammalian prion amyloids. *Cell 121*, 63−72.
(15) Jain, S., and Udgaonkar, J. B. (2008) Evidence for stepwise formation of amyloid fibrils by the mouse prion protein. *J. Mol. Biol. 382*, 1228−1241.
(16) Singh, J., and Udgaonkar, J. B. (2013) Dissection of conformational conversion events during prion amyloid fibril formation using hydrogen exchange and mass spectrometry. *J. Mol. Biol. 425*, 3510−3521.
(17) Jones, E. M., Surewicz, K., and Surewicz, W. K. (2006) Role of N-terminal familial mutations in prion protein fibrillization and prion amyloid propagation in vitro. *J. Biol. Chem. 281*, 8190−8196.
(18) Novitskaya, V., Bocharova, O. V., Bronstein, I., and Baskakov, I. V. (2006) Amyloid fibrils of mammalian prion protein are highly toxic to cultured cells and primary neurons. *J. Biol. Chem. 281*, 13828−13836.
(19) Simoneau, S., Rezaei, H., Salès, N., Kaiser-Schulz, G., Lefebvre-Roque, M., Vidal, C., Fournier, J.-G., Comte, J., Wopfner, F., Grosclaude, J., Schätzl, H., and Lasmézas, C. I. (2007) In vitro and in vivo neurotoxicity of prion protein oligomers. *PLoS Pathog. 3*, No. e125.
(20) Legname, G., Baskakov, I. V., Nguyen, H.-O. B., Riesner, D., Cohen, F. E., DeArmond, S. J., and Prusiner, S. B. (2004) Synthetic mammalian prions. *Science 305*, 673−676.
(21) Wang, F., Wang, X., Yuan, C.-G., and Ma, J. (2010) Generating a prion with bacterially expressed recombinant prion protein. *Science 327*, 1132−1135.
(22) Castilla, J., Saá, P., Hetz, C., and Soto, C. (2005) In vitro generation of infectious scrapie prions. *Cell 121*, 195−206.
(23) Come, J. H., Fraser, P. E., and Lansbury, P. T. (1993) A kinetic model for amyloid formation in the prion diseases: importance of seeding. *Proc. Natl. Acad. Sci. U. S. A. 90*, 5959−5963.
(24) Griffith, J. S. (1967) Self-replication and scrapie. *Nature 215*, 1043.
(25) Sabareesan, A., and Udgaonkar, J. B. (2014) Amyloid fibril formation by the chain B subunit of monellin occurs by a nucleation-dependent polymerization mechanism. *Biochemistry 53*, 1206−1217.
(26) Ramachandran, G., and Udgaonkar, J. B. (2012) Evidence for the existence of a secondary pathway for fibril growth during the aggregation of tau. *J. Mol. Biol. 421*, 296−314.
(27) Wood, S. J., Wypych, J., Steavenson, S., Louis, J.-C., Citron, M., and Biere, A. L. (1999) α-Synuclein Fibrillogenesis Is Nucleation-dependent implications for the pathogenesis of Parkinson's disease. *J. Biol. Chem. 274*, 19509−19512.
(28) Bhattacharyya, A. M., Thakur, A. K., and Wetzel, R. (2005) Polyglutamine aggregation nucleation: Thermodynamics of a highly unfavorable protein folding reaction. *Proc. Natl. Acad. Sci. U. S. A. 102*, 15400−15405.
(29) Xue, W.-F., Homans, S. W., and Radford, S. E. (2008) Systematic analysis of nucleation-dependent polymerization reveals new insights into the mechanism of amyloid self-assembly. *Proc. Natl. Acad. Sci. U. S. A. 105*, 8926−8931.
(30) Jarrett, J. T., and Lansbury, P. T. (1993) Seeding "one-dimensional crystallization" of amyloid: a pathogenic mechanism in Alzheimer's disease and scrapie? *Cell 73*, 1055−1058.
(31) Kundu, B., Maiti, N. R., Jones, E. M., Surewicz, K. A., Vanik, D. L., and Surewicz, W. K. (2003) Nucleation-dependent conformational conversion of the Y145Stop variant of human prion protein: structural clues for prion propagation. *Proc. Natl. Acad. Sci. U. S. A. 100*, 12069−12074.
(32) Coleman, B. M., Harrison, C. F., Guo, B., Masters, C. L., Barnham, K. J., Lawson, V. A., Hill, A. F., and Caughey, B. W. (2014) Pathogenic mutations within the hydrophobic domain of the prion protein lead to the formation of protease-sensitive prion species with increased lethality. *J. Virol. 88*, 2690−2703.
(33) Solomon, I. H., Huettner, J. E., and Harris, D. A. (2010) Neurotoxic mutants of the prion protein induce spontaneous ionic currents in cultured cells. *J. Biol. Chem. 285*, 26719−26726.
(34) Groveman, B. R., Kraus, A., Raymond, L. D., Dolan, M. A., Anson, K. J., Dorward, D. W., and Caughey, B. (2015) Charge Neutralization of the Central Lysine Cluster in Prion Protein (PrP) Promotes PrPSc-like Folding of Recombinant PrP Amyloids. *J. Biol. Chem. 290*, 1119−1128.
(35) Liemann, S., and Glockshuber, R. (1999) Influence of amino acid substitutions related to inherited human prion diseases on the thermodynamic stability of the cellular prion protein. *Biochemistry 38*, 3258−3267.
(36) Singh, J., and Udgaonkar, J. B. (2015) Structural effects of multiple pathogenic mutations suggest a model for the initiation of misfolding of the prion protein. *Angew. Chem., Int. Ed. 127*, 7639−7643.
(37) Agashe, V. R., and Udgaonkar, J. B. (1995) Thermodynamics of denaturation of barstar: evidence for cold denaturation and evaluation of the interaction with guanidine hydrochloride. *Biochemistry 34*, 3286−3299.
(38) Moulick, R., and Udgaonkar, J. B. (2014) Thermodynamic characterization of the unfolding of the prion protein. *Biophys. J. 106*, 410−420.
(39) Horcas, I., Fernandez, R., Gomez-Rodriguez, J. M., Colchero, J., Gomez-Herrero, J., and Baro, A. M. (2007) WSXM: A software for scanning probe microscopy and a tool for nanotechnology. *Rev. Sci. Instrum. 78*, 013705−013708.
(40) Nielsen, L., Khurana, R., Coats, A., Frokjaer, S., Brange, J., Vyas, S., Uversky, V. N., and Fink, A. L. (2001) Effect of environmental factors on the kinetics of insulin fibril formation: elucidation of the molecular mechanism. *Biochemistry 40*, 6036−6046.
(41) Bishop, M. F., and Ferrone, F. A. (1984) Kinetics of nucleation-controlled polymerization. A perturbation treatment for use with a secondary pathway. *Biophys. J. 46*, 631−644.
(42) Sabareesan, A., and Udgaonkar, J. B. (2016) Pathogenic Mutations within the Disordered Palindromic Region of the Prion Protein Induce Structure Therein and Accelerate the Formation of Misfolded Oligomers. *J. Mol. Biol. 428*, 3935−3947.
(43) Swietnicki, W., Petersen, R. B., Gambetti, P., and Surewicz, W. K. (1998) Familial mutations and the thermodynamic stability of the recombinant human prion protein. *J. Biol. Chem. 273*, 31048−31052.
(44) Giehm, L., and Otzen, D. E. (2010) Strategies to increase the reproducibility of protein fibrillization in plate reader assays. *Anal. Biochem. 400*, 270−281.

DOI: 10.1021/acs.biochem.7b00894
Biochemistry 2017, 56, 5931−5942

(45) Kumar, S., and Udgaonkar, J. B. (2009) Conformational conversion may precede or follow aggregate elongation on alternative pathways of amyloid protofibril formation. *J. Mol. Biol. 385*, 1266−1276.
(46) Flyvbjerg, H., Jobs, E., and Leibler, S. (1996) Kinetics of self-assembling microtubules: an "inverse problem" in biochemistry. *Proc. Natl. Acad. Sci. U. S. A. 93*, 5975−5979.
(47) Frieden, C. (2007) Protein aggregation processes: In search of the mechanism. *Protein Sci. 16*, 2334−2344.
(48) Kumar, S., and Udgaonkar, J. B. (2009) Structurally Distinct Amyloid Protofibrils Form on Separate Pathways of Aggregation of a Small Protein. *Biochemistry 48*, 6441−6449.
(49) Oosawa, F., and Kasai, M. (1962) A theory of linear and helical aggregations of macromolecules,. *J. Mol. Biol. 4*, 10−21.
(50) Soreghan, B., Kosmoski, J., and Glabe, C. (1994) Surfactant properties of Alzheimer's A beta peptides and the mechanism of amyloid aggregation. *J. Biol. Chem. 269*, 28551−28554.
(51) Harper, J. D., and Lansbury, P. T., Jr (1997) Models of amyloid seeding in Alzheimer's disease and scrapie: mechanistic truths and physiological consequences of the time-dependent solubility of amyloid proteins. *Annu. Rev. Biochem. 66*, 385−407.
(52) Chen, S., Ferrone, F. A., and Wetzel, R. (2002) Huntington's disease age-of-onset linked to polyglutamine aggregation nucleation. *Proc. Natl. Acad. Sci. U. S. A. 99*, 11884−11889.
(53) Powers, E. T., and Powers, D. L. (2008) Mechanisms of Protein Fibril Formation: Nucleated Polymerization with Competing Off-Pathway Aggregation. *Biophys. J. 94*, 379−391.
(54) Meisl, G., Kirkegaard, J. B., Arosio, P., Michaels, T. C., Vendruscolo, M., Dobson, C. M., Linse, S., and Knowles, T. P. (2016) Molecular mechanisms of protein aggregation from global fitting of kinetic models. *Nat. Protoc. 11*, 252.
(55) Ferrone, F. (1999) Analysis of protein aggregation kinetics. In *Methods in Enzymology*, pp 256−274, Academic Press, New York.
(56) Ferrone, F. A., Kheterpal, I., and Wetzel, R. (2006) Nucleation: The Connections Between Equilibrium and Kinetic Behavior. In *Methods in Enzymology*, pp 285−299, Academic Press, New York.
(57) Chiti, F., and Dobson, C. M. (2006) Protein misfolding, functional amyloid, and human disease. *Annu. Rev. Biochem. 75*, 333−366.
(58) Colon, W., and Kelly, J. W. (1992) Partial denaturation of transthyretin is sufficient for amyloid fibril formation in vitro. *Biochemistry 31*, 8654−8660.
(59) Khare, S. D., Caplow, M., and Dokholyan, N. V. (2004) The rate and equilibrium constants for a multistep reaction sequence for the aggregation of superoxide dismutase in amyotrophic lateral sclerosis,. *Proc. Natl. Acad. Sci. U. S. A. 101*, 15094−15099.
(60) Jahn, T. R., Parker, M. J., Homans, S. W., and Radford, S. E. (2006) Amyloid formation under physiological conditions proceeds via a native-like folding intermediate. *Nat. Struct. Mol. Biol. 13*, 195−201.
(61) Honda, R. P., and Kuwata, K. (2017) The native state of prion protein (PrP) directly inhibits formation of PrP-amyloid fibrils in vitro,. *Sci. Rep. 7*, 562.
(62) Collins, S. R., Douglass, A., Vale, R. D., and Weissman, J. S. (2004) Mechanism of prion propagation: amyloid growth occurs by monomer addition. *PLoS Biol. 2*, No. e321.
(63) Hölscher, C., Delius, H., and Bürkle, A. (1998) Overexpression of nonconvertible PrP c Δ114−121 in scrapie-infected mouse neuroblastoma cells leads to trans-dominant inhibition of wild-type PrP Sc accumulation. *J. Virol. 72*, 1153−1159.
(64) Sengupta, I., Bhate, S. H., Das, R., and Udgaonkar, J. B. (2017) Salt-Mediated Oligomerization of the Mouse Prion Protein Monitored by Real-Time NMR. *J. Mol. Biol. 429*, 1852−1872.
(65) Lührs, T., Zahn, R., and Wüthrich, K. (2006) Amyloid formation by recombinant full-length prion proteins in phospholipid bicelle solutions. *J. Mol. Biol. 357*, 833−841.
(66) Nyström, S., Mishra, R., Hornemann, S., Aguzzi, A., Nilsson, K. P. R., and Hammarström, P. (2012) Multiple substitutions of methionine 129 in human prion protein reveal its importance in the amyloid fibrillation pathway. *J. Biol. Chem. 287*, 25975−25984.
(67) Wogulis, M., Wright, S., Cunningham, D., Chilcote, T., Powell, K., and Rydel, R. E. (2005) Nucleation-dependent polymerization is an essential component of amyloid-mediated neuronal cell death. *J. Neurosci. 25*, 1071−1080.
(68) Nonaka, T., Watanabe, S. T., Iwatsubo, T., and Hasegawa, M. (2010) Seeded Aggregation and Toxicity of α-Synuclein and Tau CELLULAR MODELS OF NEURODEGENERATIVE DISEASES. *J. Biol. Chem. 285*, 34885−34898.
(69) Jan, A., Adolfsson, O., Allaman, I., Buccarello, A.-L., Magistretti, P. J., Pfeifer, A., Muhs, A., and Lashuel, H. A. (2011) Aβ42 neurotoxicity is mediated by ongoing nucleated polymerization process rather than by discrete Aβ42 species. *J. Biol. Chem. 286*, 8585−8596.
(70) Slepko, N., Bhattacharyya, A. M., Jackson, G. R., Steffan, J. S., Marsh, J. L., Thompson, L. M., and Wetzel, R. (2006) Normal-repeat-length polyglutamine peptides accelerate aggregation nucleation and cytotoxicity of expanded polyglutamine proteins. *Proc. Natl. Acad. Sci. U. S. A. 103*, 14367−14372.
(71) Perutz, M. F., and Windle, A. (2001) Cause of neural death in neurodegenerative diseases attributable to expansion of glutamine repeats. *Nature 412*, 143−144.
(72) Asakura, S., and Oosawa, F. (1975) *Thermodynamics of the Polymerization of Protein*, Academic Press, London.

DOI: 10.1021/acs.biochem.7b00894
Biochemistry 2017, 56, 5931−5942